CHEMICAL ENGINEERING TRANSACTIONS
VOL. 84, 2021
A publication of AIDIC
The Italian Association of Chemical Engineering
Online at www.cetjournal.it
Guest Editors: Paolo Ciambelli, Luca Di Palma

ISBN 978-88-95608-82-2; **ISSN** 2283-9216
DOI: 10.3303/CET2184005

Improved Nanocomposite Photoanodes by Controlled Deposition of g-C_3N_4 on Titania Nanotube Ordered Films

Rosalba Passalacqua*, Salvatore Abate, Siglinda Perathoner, Gabriele Centi

Departments of ChiBioFarAM and MIFT, University of Messina, ERIC aisbl and INSTM/CASPE, Viale F. Stagno d'Alcontres 31, Messina 98166, Italy
rpassalacqua@unime.it

The photoelectrocatalytic properties of TiO_2 nanotube ordered films (TiNT) could be enhanced by decorating them with graphitic-C_3N_4. The g-C_3N_4/TiNT heterojunctions have been successfully prepared using a facile and direct chemical vapor deposition method. By controlling type and amount of utilized nitrogen precursor, it is possible to tune the properties of the resulting nanocomposites. Under light irradiation the photoelectrocatalytic activity of the fabricated g-C_3N_4/TiNT heterojunctions is about 4.7 times than that of bare TiNT, due to their better separation capability of photogenerated charges and wider optical absorption. Characterization by XRD, XPS, UV-Vis DRS and chronoamperometry under simulated sunlight, evidence the relations between the method of preparation and the features of the samples, revealing the high potential of these nanocomposites.

1. Introduction

The design of new materials with improved properties is at the centre of growing attention in developing novel solutions to address challenges opened by the energy transition. In this context the development of improved, but robust photoanodes for photoelectrocatalytic (PEC) applications remains a challenge, notwithstanding the large scientific effort. TiO_2, despite a band gap in the near UV, continues to be one of the main nanomaterials used in photoanodes, for its characteristics and robustness, even if its visible activity should be improved (Bai et al., 2014). The properties of nanocarbons as photoactive materials (Perathoner et al., 2017) and their feasible use for band gap engineering suggest the interest in investigating nanocomposites derived by coupling metal-free organic semiconductors such as graphitic carbon nitride (g-C_3N_4) with nanostructured films of ordered arrays of vertically-aligned 1-D titania nanotubes obtained by anodization. The studies on these materials are limited and generally in relation to their use in dye-sensitized solar cell (Mohammadi et al., 2020). A series of nanocomposite samples was obtained from different nitrogen precursors (melamine, urea and a mix 1:1 melamine/urea) on TiNT. The samples were prepared and characterized by a set of complementary techniques to correlate their photocatalytic behaviour with the surface structure and composition. These nanocomposites show a good stability and can be applied both in environmental remediation uses, such as removal of toxic organic contaminants, and as advanced nanostructured photoanode in solar energy conversion systems, particularly in PEC-type devices to produce solar fuels (Lanzafame et al., 2017). Note that the nanostructure of these photoanodes allows developing compact-type of PEC cells without using a bulk-electrolyte, a solution which improves performances, product recovery and cell scalability (Perathoner et al., 2016). Besides these applications, the samples have been recently utilized, by our research group, as cathodic materials for the electrocatalytic reduction of oxalic acid (De Luca et al., 2021) with promising results.

2. Experimental

2.1. g-C_3N_4/TiNT nanocomposite preparation

The g-C_3N_4/TiNT nanocomposites were prepared in a two-step process. In the first step the synthesis of

Paper Received: 3 July 2020; Revised: 14 November 2020; Accepted: 9 February 2021
Please cite this article as: Passalacqua R., Abate S., Perathoner S., Centi G., 2021, Improved Nanocomposite Photoanodes by Controlled Deposition of G-c3n4 on Titania Nanotube Ordered Films, Chemical Engineering Transactions, 84, 25-30 DOI:10.3303/CET2184005

highly ordered TiO_2 nanotube arrays (TiNT) was performed, by controlled anodic oxidation (AO) of a titanium foil (Passalacqua et al., 2014), in the second step the nanotubes decoration with the g-C_3N_4 layer (see Figure 1).

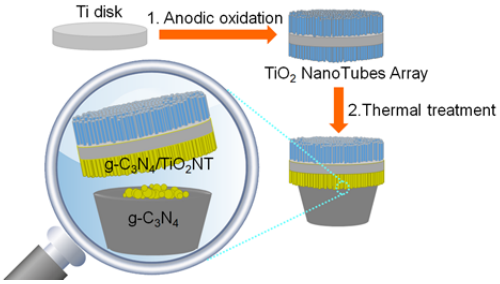

Figure1: Scheme of the two-step synthesis of g-C_3N_4/TiNT nanocomposites

In a typical preparation procedure, a Ti disc (0.025 mm thick, 35 mm dia., 99.96 % purity, Alfa Aesar) was cleaned by sonication in deionized water, acetone and isopropyl alcohol, sequentially. Then, it was dried in air stream, and finally anodized at room temperature (rt) in a stirred electrochemical bath containing ethylene glycol, 0.3 wt. % NH_4F and 2 vol. % H_2O. The AO was carried out at 50 V for 1h, in a Teflon cell having a two-electrode setup connected to a DC power supply (Agilent E3612A) and equipped with a multimeter (Keithley2000/E model) for recording the current signal. The Ti disc and a glassy carbon rod served as working electrode and counter electrode, respectively. Then, the TiNT was rinsed with water and dried in air (Passalacqua et al., 2015). In the second step it was realized the decoration of TiNT with g-C_3N_4 patches by a direct chemical vapor deposition (CVD) method using melamine (Sun et al., 2016), urea or a 1:1 mixture of melamine-urea as precursor. Briefly, a certain amount of precursor (6, 12, 18 or $24 \cdot 10^{-3}$ mol) was put in a cleaned ceramic crucible, and the anodized disc used as a cover. Then the crucible was heated (heating and cooling rate 5 ºC/min) in a muffle in air at 550 ºC for 3h. After the treatment, the g-C_3N_4 polymer was successfully deposited onto top of the crystalline structure of TiO_2 nanotubes, while some yellow g-C_3N_4 powder was also obtained in the crucible. This last product was ground to a fine powder before analysis. The proportion between g-C_3N_4 and TiO_2 nanotubes in the composites was adjusted by varying the starting amount of precursor (melamine, urea or 1:1 melamine-urea mix) in the crucible.
The investigated samples and their characteristics of preparation are collected in Table 1.

Table 1: Investigated samples and their characteristics of preparation

Sample name	Chemical components	AO parameters	g-C_3N_4 precursor
TiNT	TiO_2/Ti	50 V; 1h	---
TiNTM6	g-C_3N_4-TiO_2/Ti	50 V; 1h	Melamine $6 \cdot 10^{-3}$ mol
TiNTM12	g-C_3N_4-TiO_2/Ti	50 V; 1h	Melamine $12 \cdot 10^{-3}$ mol
TiNTM18	g-C_3N_4-TiO_2/Ti	50 V; 1h	Melamine $18 \cdot 10^{-3}$ mol
TiNTM24	g-C_3N_4-TiO_2/Ti	50 V; 1h	Melamine $24 \cdot 10^{-3}$ mol
TiNTU6	g-C_3N_4-TiO_2/Ti	50 V; 1h	Urea $6 \cdot 10^{-3}$ mol
TiNTU12	g-C_3N_4-TiO_2/Ti	50 V; 1h	Urea $12 \cdot 10^{-3}$ mol
TiNTU18	g-C_3N_4-TiO_2/Ti	50 V; 1h	Urea $18 \cdot 10^{-3}$ mol
TiNTU24	g-C_3N_4-TiO_2/Ti	50 V; 1h	Urea $24 \cdot 10^{-3}$ mol
TiNTMU6	g-C_3N_4-TiO_2/Ti	50 V; 1h	1:1 Melamine-Urea $6 \cdot 10^{-3}$ mol
TiNTMU12	g-C_3N_4-TiO_2/Ti	50 V; 1h	1:1 Melamine-Urea $12 \cdot 10^{-3}$ mol
TiNTMU18	g-C_3N_4-TiO_2/Ti	50 V; 1h	1:1 Melamine-Urea $18 \cdot 10^{-3}$ mol
TiNTMU24	g-C_3N_4-TiO_2/Ti	50 V; 1h	1:1 Melamine-Urea $24 \cdot 10^{-3}$ mol

2.2. Characterization

Crystallographic phases and structure of the g-C_3N_4/TiNT samples were investigated by X-ray diffraction. The XRD spectra were recorded with a Philips X'Pert 3710 instrument, using Cu Kα radiation (λ = 0.154178 nm, 30 kV and 40 mA) under a glancing angle of 2° or lower. Data were collected over a 2θ range of 10-80°.

A Bruker D2 Phaser desktop X-ray diffraction system operating with the conventional Bragg-Brentano geometry was used to analyse the yellow powders of g-C_3N_4 collected in the crucible together with the composites after the thermal condensation treatment. Diffraction peak identification was made based on the JCPDS database of reference compounds. A Phenom benchtop SEM was used for acquiring the micrographs of the g-C_3N_4 powders. Oxidation states and surface chemical composition of the composites were acquired by XPS measurements. XPS spectra were recorded using a PHI VersaProbe II analyser (Physical Electronics). The results were analysed by using the Multipack (Matlab) software. XPS peaks position was referred to graphite carbon C 1s signal, whose peak energy was set at 284.8 eV for calibration.
The optical absorption properties were investigated using UV–vis diffuse reflectance spectra (UV-vis DRS) recorded by a JASCO V570 spectrometer equipped with an integrating sphere for solid samples. Chronoamperometry experiments were carried out, at rt under frontal lighting, with a photo-electrochemical cell having a standard three-electrode set-up, on a 2049 AMEL potentiostat-galvanostat equipped with a Pt wire as the counter, a saturated Ag/AgCl electrode as the reference, and the prepared samples as the working electrode. The tests were performed in 0.5 M Na_2SO_4 solution purged with N_2, at 0.1 or 0 V vs Ag/AgCl. The light source was a 300 W Xe arc lamp (Lot-Oriel) equipped with a set of lenses for light collection and focusing, a water filter to eliminate the infrared radiation and a set of filters to select the desired wavelength range for evaluating the photo-response in the ultraviolet or visible region of the electromagnetic spectrum. The working electrode was illuminated from the front and an AM1.5G filter simulating solar radiation was used, whereas to cut wavelength below 480 and 280 nm the LSZ179 (UVB/C blocking filter 320-480 nm, 700-4400 nm) and LSZ178 (UVC blocking filter 280-4400 nm) optical filters (Lot-Oriel) were used, respectively.

3. Results and discussion

The preparation of the g-C_3N_4/TiNT nanocomposites requires a single synthesis step, in which in addition to the pyrolysis and condensation of the nitrogen precursors, the crystallization of the titania nanotubes film, obtained in amorphous form after the initial AO phase, occurs (see Figure 1). During the thermal treatment, the tris-s-triazine forms via melamine rearrangements at round 390 ºC while condensation of this unit to the final polymeric C_3N_4 species occurs at around 520 ºC (Thomas et al., 2008).
Data obtained by XRD confirm the formation of the characteristic graphite-like stacking of C_3N_4 layers in all the prepared samples in agreement with earlier literature (Liao et al, 2012; Martha et al. 2013). The pristine nanotube arrays consist mainly of anatase (Passalacqua et al., 2015). The rutile phase is present in low amount, XRD recorded in glancing angle mode show that it is preferentially located at the interface between the TiO_2 nanotubes and the metallic Ti. In fact, as observed in the pattern of the TiNTMU18, by reducing the incident angle from 2.0 to 0.2° the diffraction peaks at ~ 27.5° and 40° disappear. Therefore, these peaks can be attributable to the rutile phase located at the interface between the TiO_2 nanotubes and the metallic Ti.
The X-ray diffraction patterns are shown in Figure 2. Two peaks are observed in the XRD patterns for bare g-C_3N_4 powders prepared from melamine, urea (not reported) and equimolar ratio of melamine/urea. The first peak, found at 13.08º, corresponds to the in-plane structural packing motif of tri-s-triazine ring; it is indexed to (100) diffraction plane for graphitic materials (Thomas et al., 2008). The strongest peak at 27.36º assigned as (002) diffraction plane is related to the interlayer stacking of the conjugated aromatic system. In the case of graphitic C_3N_4 prepared from MU1:1, the peaks are slightly shifted towards lower angles, 12.92º and 27.26º, with significant broadening and a slight decrease in the overall intensity. This shifted peak position indicates an increment in both the in-plane nitride pores and the interlayer distance between the conjugated aromatic system (Martha et al., 2013) and it corresponds to a g-C_3N_4 MU derived species with conjugated aromatic layers well separated compared to the single precursor samples, TiNTM18 and TiNTU18, which results in superior photocatalytic activity.
In the diffraction pattern of the composites the main peak at 25.38º, 25.42º and 25.34º can be indexed to the (101) crystal plane of anatase (JCPDS file No. 21-1272) while the reflection of lower intensity appearing at 2Θ values of 27.50º, 27.54º, and 27.50º, for M-, U- and MU- derivatives, respectively, can be indexed to the (110) crystal plane of rutile (JCPDS card No. 21-1276).
Rutile diffraction signal and graphitic carbon signal fall almost at the same value of 2Θ, so it is possible an overlap of the two diffraction peaks. An in-dept investigation revealed that the peak of rutile is located at 27.50º and that of the g-C_3N_4 system, related to the characteristic peak of the (002) crystal plane, is observed at 27.36º. Layered g-C_3N_4 structures were highlighted by SEM micrographs (see Figure 2e). They are also visible in the bulk powder reported in Figure 2d. Interestingly, the g-C_3N_4 grew uniformly on the TiO_2 nanotubes without damage the intrinsic structure of TiO_2 nanotube matrix (see Figure 2e).
X-ray photoelectron spectroscopy (XPS) was performed to analyze oxidation states and surface chemical composition of all the prepared samples. The survey spectra (not reported) confirm that the prepared samples

are composed of the C, N, Ti and O elements. C 1s XPS spectrum of TiNTM24, displayed in Figure 3a, shows three main peaks indicating that carbon has been found in three diverse chemical states. The peak at 284.59 eV can be ascribed to the adventitious carbon (sp^2 C–C bonds), that at 288.73 eV to the sp^3 carbon atom in the N–C=N group (Han et al. 2014), another peak was also detected at 286.03 eV, attributing to the sp^2 carbon atoms bonded to N inside the aromatic units (Zhou et al. 2012) or to C–OH (Liu et al. 2018). The last two peaks are typical features of the tri-s-triazine units in CNs.

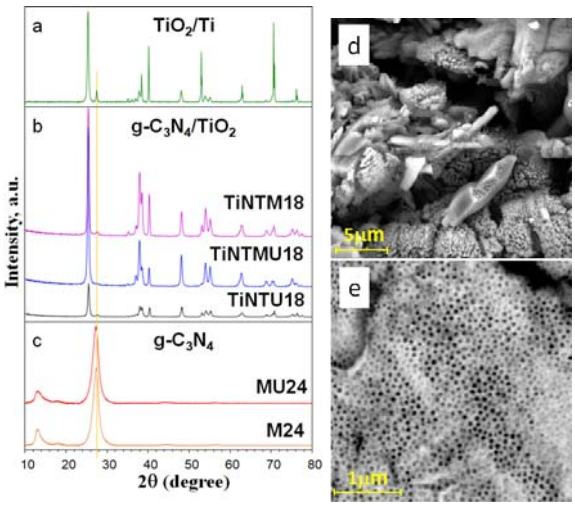

Figure 2: XRD profiles of a) TiO_2/Ti support; b) Melamine, Melamine-Urea and Urea derived composites recorded with a 2 ° glancing angle; c) CN_x powders recovered in the crucible; d) SEM micrograph of g-C_3N_4 powder obtained from $18 \cdot 10^{-3}$ mol melamine precursor; e) SEM micrograph of TiNTM18 sample

The N 1s signal is characterized by a low intensity; this feature is commonly observed in such systems (Sun et al. 2016, Liu et al. 2018). For the discussion about the assignment of the three N signals see De Luca et al., 2021. The XPS results concerning N1s and Ti2p signals confirm not only the existence of CNs species in the prepared composites but also the interaction between the two components and ultimately the successful preparations of the heterojunctions (Chang et al. 2014). Moreover, note that for the Ti2p core level spectrum of samples TiNTMU18, TiNTM6 and TiNTM18, a shift toward higher binding energy (BE) was observed. Interestingly, TiNTMU18 and TiNTM6 are among the samples that showed a better photocurrent behavior.

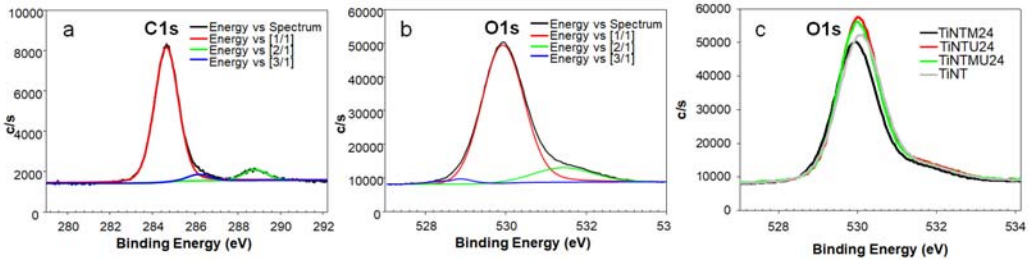

Figure 3: XPS spectra of a) C 1s core level of TiNTM24, b) O 1s core level of TiNTM24, c) C 1s core level of TiNTM24, TiNTU24, TiNTMU24 and TiNT reference

The O 1s spectrum of both pure TiO_2 sample and TiNTM24 sample can be fitted into three peaks, with signals at 528.60, 530.07 and 531.49 eV for the reference and at 528.59, 529.93 and 531.44 eV for the g-C_3N_4 composite. The main peaks at around 529.93 eV and 531.44 eV can be attributed to O atoms in Ti–O–Ti (Zhou et al. 2012) and surface OH, respectively. In Figure 3c the small shift to lower BE observed for the composites, suggests the incorporation of N in TiO_2 lattice as previously reported by other authors (Boonprakob et al., 2014). The optical absorption properties of g-C_3N_4/TiNTs were investigated using UV-vis diffuse reflectance spectra (UV-vis DRS) (see Figure 4). All the samples show a broad absorption shifted towards visible region due to the presence of g-C_3N_4. The estimated optical band gaps (E_g) for pure g-C_3N_4 (powders obtained with TiNTMU24 and TiNTM24) and for the TiNT support are 2.70 and 3.13 eV, with the absorption edges at about 410 and 440 nm, respectively. Higher E_g values have been obtained for the composites ranging between 3.15 and 3.64 eV.

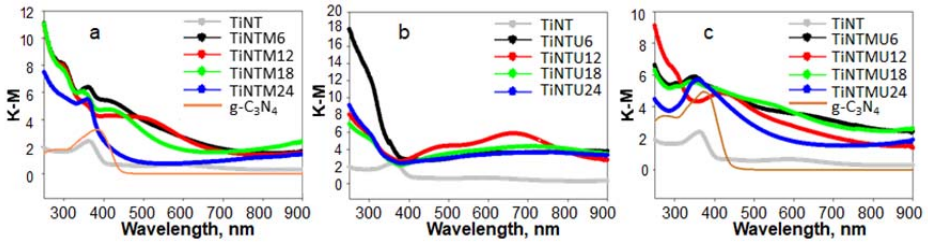

Figure 4: UV-vis DRS of reference TiNT, pure C_3N_4 (from M24 and MU24 powders), and g-C_3N_4/TiO_2 composites derived from a) melamine; b) urea; and c) 1:1 melamine-urea precursor

Potentiostatic plots, carried out by irradiation with UV–vis radiation, highlight a rapid photocurrent generation (see Figure 5). All the samples were found to be photoactive both under UV and visible light. A decrease of the initial photocurrent was observed when performing the measurements with the aid of filters blocking portions of the incident UV-vis radiation. In particular, for TiNTMU18 using the AM1.5G filter, the photocurrent response is 14.1% of the initial value obtained under the full spectrum lamp irradiation, with UVB/C LSZ179 and UVC LSZ178 filters the photocurrent reduces to 62.7% and 19.7%, respectively (see Figure 5 b).
The observed photocurrent responses were significantly different depending on the composition of the sample, with a higher density of photocurrent for MU18 compared to those of single precursor derived composites. Moreover, increasing the precursor content from 6 to $18 \cdot 10^{-3}$ mol an increase of photocurrent was generally observed, while for the samples with the higher precursor concentration, a lowering in photocurrent response was noted. This trend is probably indicative of a saturation effect compatible with a thick g-C_3N_4 layer covering the TiO_2 nanotube surface (see UV-vis DRS in Figure 4).
ON/OFF illumination of the photoelectrodic sample shows an instantaneous rise in photocurrent and quick recovery to the original photocurrent through multiple ON/OFF cycles and after five cycles of on/off switching, the signal stabilizes (see Figure 5a). The monitoring during discontinuous illumination revealed stability and reproducibility of the photocurrent in all the tested samples.

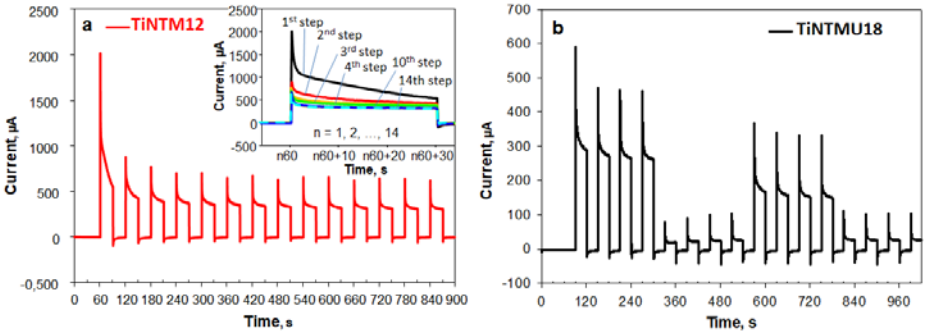

Figure 5: Chronoamperometric plot of a) TiNTM12 showing the changes in the photocurrent response under irradiation. The insert exhibits the modification of the current profile when switching from the first on/off cycle to the fourteenth cycle (highlighting the stability of the signal after five cycles); b) TiNTMU18 under different irradiations (full Xe spectrum, AM1.5G, UVB/C and UVC blocking filters)

The photocurrents in samples obtained from different concentrations of the same precursor decrease as follows:
TiNTM12 > TiNTM6 > TiNTM18 > TiNTM24
TiNTU18 > TiNTU12 > TiNTU6 > TiNTU24
TiNTMU18 > TiNTMU12 > TiNTMU24 ≥ TiNTMU6
for melamine, urea and 1:1 melamine/urea, respectively.

4. Conclusions

In summary, we have demonstrated the fabrication of carbon nitride materials with tuneable properties depending on the composition and amount of the starting nitrogen precursor.
The resulting composites exhibit in all cases improved optical absorption in the visible region and a better photoelectrochemical response in comparison to the TiNT single component**.** The increments of photocurrent are at least double and up to 4.7 times than that of bare TiO_2. The most stable and intense current was

observed for TiNTMU18 whereas TiNTM12 and TiNTU18 after the first four on-off cycles show signals of similar form and intensity even if for the TiNTM12 sample was initially recorded the highest increment of current under irradiation.
Present trends indicate that this type of hybrid materials having enhanced properties can be successfully used in the field of photocatalysis.

Acknowledgments

This research has received funding from the MIUR under the PRIN2017 programme (project CO_2 ONLY) and from the European Union's HORIZON2020 research and innovation program (OCEAN agreement ID 767798).

References

Bai Y., Mora-Sero I., De Angelis F., Bisquert J., Wang P., 2014, Titanium dioxide nanomaterials for photovoltaic applications, Chemical Reviews, 114, 10095-10130.

Boonprakob N., Wetchakun N., Phanichphant S., Waxler D., Sherrell P., Nattestad A., Chen J., Inceesungvorn B., 2014, Enhanced visible-light photocatalytic activity of g-C_3N_4/TiO_2 films, Journal of Colloid and Interface Science, 417, 402–409.

Chang F., Zhang J., Xie Y., Chen J., Li C., Wang J., Luo J., Deng B., Hu X., 2014, Fabrication, characterization, and photocatalytic performance of exfoliated g-C_3N_4–TiO_2 hybrids. Applied Surface Science, 311, 574–581.

De Luca F., Passalacqua R., Abate S., Abramo F.P., Perathoner S., Centi G., 2021, Graphitic-C_3N_4/TiO_2 Nanotube Array as Cathodic Materials for the Electrocatalytic Reduction of Oxalic Acid, Chemical Engineering Transactions, 84, accepted.

Han C., Wang Y., Lei Y., Wang B., Wu N., Shi Q., Li Q., 2014, In situ synthesis of graphitic-C_3N_4 nanosheet hybridized N-doped TiO_2 nanofibers for efficient photocatalytic H_2 production and degradation, Nano Research DOI 10.1007/s12274-014-0600-2.

Lanzafame P., Abate S., Ampelli C., Genovese C., Passalacqua R., Centi G., Perathoner S., 2017, Beyond Solar Fuels: Renewable Energy-Driven Chemistry, ChemSusChem, 10, 4409-4419.

Liao G., Chen S., Quan X., Yu H., Zhao H., 2012, Graphene oxide modified g-C_3N_4 hybrid with enhanced photocatalytic capability under visible light irradiation, Journal of Materials Chemistry, 22, 2721–2726.

Liu C., Wang F., Zhang J., Wang K., Qiu Y., Liang Q., Chen Z., 2018, Efficient Photoelectrochemical Water Splitting by g-C_3N_4/TiO_2 Nanotube Array Heterostructures, Nano-Micro Letters, 10:37.

Martha S., Nashima A., Parida K.M., 2013, Facile synthesis of highly active g-C_3N_4 for efficient hydrogen production under visible light. Journal of Materials Chemistry A, 1, 7816–7824.

Mohammadi I., Zeraatpisheh F., Ashiri E., Abdi K., 2020, Solvothermal synthesis of g-C_3N4 and ZnO nanoparticles on TiO_2 nanotube as photoanode in DSSC, International Journal of Hydrogen Energy, 45, 18831-18839.

Passalacqua R., Ampelli C., Perathoner S., Centi G., 2014, Self-standing TiO_2 nanotubular membranes for sustainable production of energy, Chemical Engineering Transactions, 41, 319-324 DOI: 10.3303/CET1441054.

Passalacqua R., Perathoner S., Centi G., 2015, Use of modified anodization procedures to prepare advanced TiO_2 nanostructured catalytic electrodes and thin film materials, Catalysis Today, 251, 121–131.

Perathoner S., Ampelli C., Chen S., Passalacqua R., Su D., Centi G., 2017, Photoactive materials based on semiconducting nanocarbons – A challenge opening new possibilities for photocatalysis, Journal of Energy Chemistry, 26, 207–218.

Perathoner S., Centi G., Su D., 2016, Turning Perspective in Photoelectrocatalytic Cells for Solar Fuels, ChemSusChem, 9, 345–357.

Sun M., Fang Y., Kong Y., Sun S., Yu Z., Umar A., 2016, Graphitic carbon nitride (g-C_3N_4) coated titanium oxide nanotube arrays with enhanced photo-electrochemical performance, Dalton Transactions, 45, 12702–12709.

Thomas A., Fischer A., Goettmann F., Antonietti M., Müller J.-O., Schlögl R., Carlsson J. M., 2008, Graphitic carbon nitride materials: variation of structure and morphology and their use as metal-free catalysts, Journal of Materials Chemistry, 18, 4893–4908.

Zhou X., Jin B., Li L., Peng F., Wang H., Yub H., Fang Y., 2012, A carbon nitride/TiO_2 nanotube array heterojunction visible-light photocatalyst: synthesis, characterization, and photoelectrochemical properties, Journal of Materials chemistry, 22, 17900–17905.